JOURNAL OF MATERIALS SCIENCE 35 (2000) 4151–4157

# Precipitation characteristics of Cu-Mn-P alloy

JOON HWAN CHOI, JUNG-SOO BYUN, DONG NYUNG LEE*
*School of Materials Science and Engineering, Seoul National University, Seoul 151-742, South Korea*

The precipitates responsible for the age-hardening effect in Cu-1.11%Mn-0.28%P alloy have been studied using transmission electron microscopy (TEM). The precipitates in the aged alloy have a rod shape and a composition of $Mn_2P$ having a hexagonal structure. Their axial direction is $[0001]_p$ and is parallel to $\langle 001\rangle_m$ of copper matrix, where subscripts 'm' and 'p' signify matrix and precipitate, respectively. Orientation relationships between the precipitates and the matrix are as follows:

$$[001]_m // [0001]_p // \text{rod axis} \quad \text{and} \quad (010)_m // (13\bar{4}0)_p$$

$$[001]_m // [0001]_p // \text{rod axis} \quad \text{and} \quad (010)_m // (12\bar{3}0)_p$$



## 1. Introduction

Materials for electronic and electrical applications such as lead frames and connectors are required to have a high strength as well as a good electrical conductivity. Therefore, copper-base alloys are widely used for the applications due to their high electrical conductivity. Most of the alloys are usually of the precipitation–strengthened types and are dilutely alloyed with elements of very low solubility to preserve high levels of conductivity.

The representative precipitation-hardenable copper-base alloys for the applications are Cu-Be [1–5], Cu-Cr [6–8], Cu-Zr [9, 10], Cu-Ni-Si [11–14], Cu-Fe-P [15–18], Cu-Ni-P [19, 20], etc. The alloys are required to have very low solid solubility at the precipitation temperature to increase the strength with minimum degrading of the conductivity. Recently, Miyake *et al.* [21] have reported that addition of phosphorus to Cu-Ni alloys forms nickel phosphide precipitates, resulting in an decrease in the residual solubility to very low levels. They also reported that the addition of iron to Cu-P alloys reduced the solubility of P in Cu and the equilibrium solubility of nickel phosphide compound in copper was much lower than that of $Ni_2Si$, Be, and Ti in Cu.

Mn also reacts with P to form an intermetallic compound. We have reported that Cu-1.11%Mn-0.28%P alloy with the atomic concentration ratio of Mn to P being about 2 to 1 exhibits high strength (a tensile strength of 662MPa), good electrical conductivity (51%IACS), and good elongation (8%) and that the alloy is strengthened by hexagonal $Mn_2P$ precipitates [22].

In the present work, the shape and the growth direction of the precipitate and the orientation relationships between the precipitate and the copper matrix of the alloy have been studied using TEM. The aging temperature employed was 723 K which is an appropriate temperature for good combination of strength and conductivity.

## 2. Materials and experimental procedure

The Cu-Mn-P alloy was prepared in a high frequency induction furnace. The chemical composition of the alloy was Cu-1.11%Mn-0.28%P. The billet was homogenized at 1173 K for 12 h and hot-rolled to a thickness of 11 mm. The plate was solution-treated at 1173 K for 3 h and then water-quenched. After machining to remove surface oxide, the plate was cold-rolled to a thickness of 1 mm, annealed at 1173 K for 3 h, and then water-quenched.

A set of static aging experiments of the 1 mm thick annealed specimens was carried out at 723 K. The Vickers microhardness measurements were carried out under an indenting load of 200 g on the mechanically polished longitudinal sections of the specimens.

Thin foils for TEM examination were thinned at 25–30 V in a twin jet electropolisher using 30% nitric acid in methanol maintained at about 243 K. The TEM examinations were carried out using a Philips CM20/STEM electron microscope operating at 200 kV.

## 3. Results and discussion

### 3.1. Age-hardening behavior and precipitate morphology

The effect of aging at 723 K on the hardness of the material is shown in Fig. 1. The hardness of the alloy reached a peak after aging for 4 h and continuously decreased

* Author to whom all correspondence should be addressed.

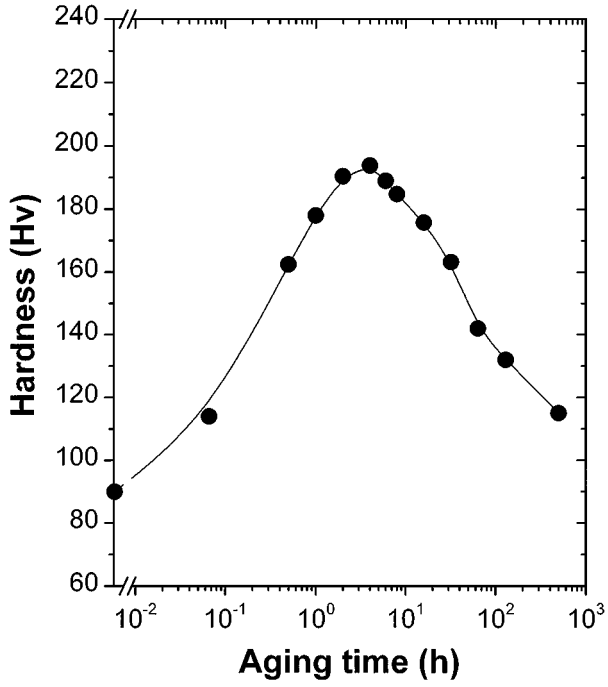


*Figure 1* Microhardness (load: 200 g) of the specimen as function of aging time at 723 K.

afterwards. Bright field images of precipitates in the alloy aged for 4 and 500 h are shown in Figs 2 and 3, respectively. The precipitates in Figs 2 and 3 appeared as rods in all of the beam directions and were elongated in the same directions.

Three sets of rod-shaped images of the precipitates can be seen at right-angles to one another in Figs 2a and 3a which were obtained from a foil oriented so that the incident beam could be parallel to the $[100]_m$ direction. The precipitates parallel to the two $\langle 100\rangle_m$ directions orthogonal to the beam direction of $[100]_m$ appear as rods and those parallel to the beam direction appear as dots.

Precipitate images were also obtained from a beam direction of $\langle 110\rangle_m$. Fig. 3b of which the zone axis is the $[\bar{1}10]_m$ direction can be obtained by a rotation through 45° about the $[001]_m$ direction in Fig. 3a. The rod-shaped precipitates parallel to the $[001]_m$ direction in Fig. 3a are not tilted by the rotation, but those parallel to the $[010]_m$ and $[100]_m$ directions in Fig. 3a appear as rods parallel to the $[110]_m$ direction in Fig. 3b. From the trace analysis, therefore, the growth direction of the rod-shaped precipitate is parallel to the $\langle 001\rangle_m$ directions of the matrix.

This is confirmed by the $[\bar{1}11]_m$ zone axis in Fig. 3c. The rods parallel to the $\langle 001\rangle_m$ directions appear to be parallel to the $\langle 112\rangle_m$ directions orthogonal to the $\langle 111\rangle$ beam direction. The precipitates in Fig. 3c having the $[\bar{1}11]_m$ zone axis were obtained by a rotation through 35.3° about the $[110]_m$ direction in Fig. 3b. They appear to be aligned parallel to three $\langle 112\rangle_m$ directions orthogonal to the beam direction. Specifically, the precipitates along the $[1\bar{1}2]_m$ directions in Fig. 3c are equivalent to those parallel to the $[001]_m$ direction in Fig. 3b while the precipitates parallel to the $[12\bar{1}]_m$ and $[211]_m$ directions in Fig. 3c are equivalent to those parallel to the $[110]_m$ direction in Fig. 3b.

The shape and the growth direction of the precipitates in Fig. 2 which was obtained from the peak-aged specimen are the same as those in Fig. 3 which was obtained from the specimen aged for 500 h.

### 3.2. Orientation relationships between the matrix and the precipitate

The precipitates in the aged alloy were identified as hexagonal $Mn_2P$ by X-ray diffraction and TEM [22]. Fig. 4a and b show selected-area diffraction patterns (SADPs) obtained from a precipitate in Fig. 3a such as the precipitate 'A' in Fig. 3d. The incident beam is parallel to the $[100]_m$ direction in the both cases. Fig. 4c and d show the analyses of the diffraction patterns in

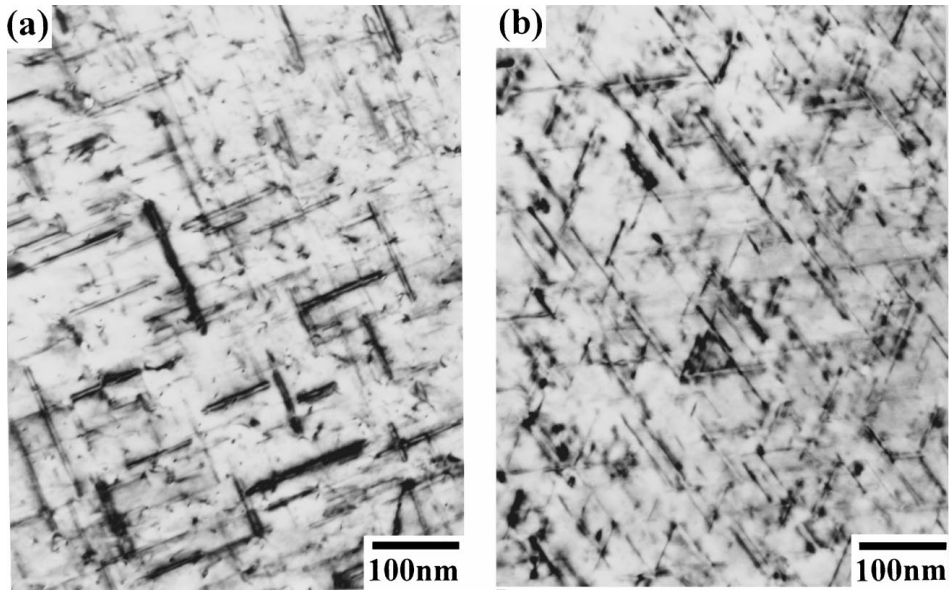


*Figure 2* Bright field TEM micrographs of specimen aged at 723 K for 4 h taken with zone axes parallel to (a) $[100]_m$ and (b) $[\bar{1}11]_m$ directions.

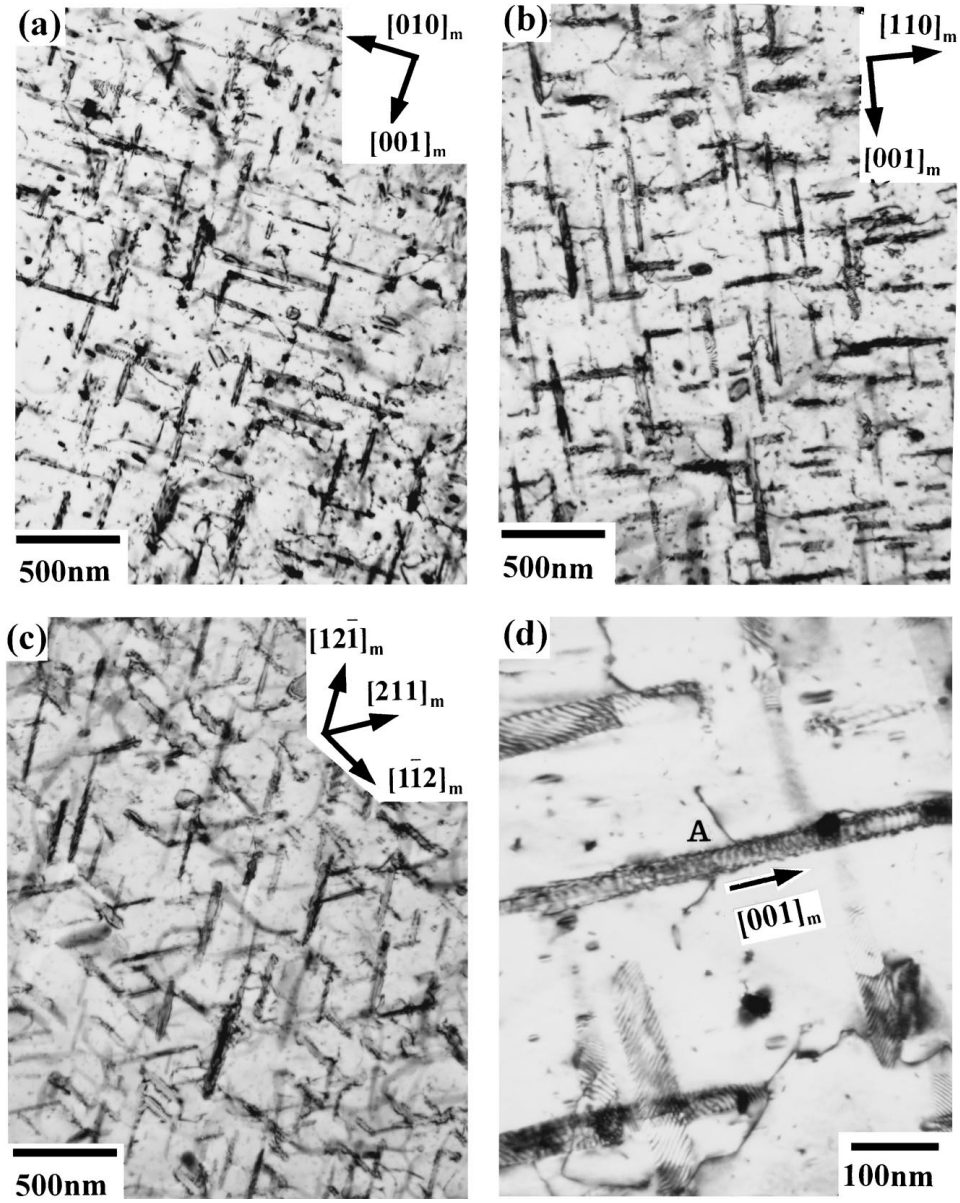


*Figure 3* Bright field TEM micrographs of specimen aged at 723 K for 500 h taken with zone axes parallel to (a) $[100]_m$, (b) $[\bar{1}10]_m$, and (c) $[\bar{1}11]$ directions. (d) Magnified image of Fig. (b).

Fig. 4a and b, respectively. The two patterns are not identical and show that the two different orientation relationships exist between the matrix and the precipitate. The precipitate spots in Fig. 4a and b contain double diffraction spots, which were represented by gray circles. In the both diffraction patterns, the $(0001)_p$ plane is parallel to the $(001)_m$ plane and orthogonal to the axial direction of the rod-shaped precipitate as shown in Fig. 3d. However, the $(020)_m$ plane in Fig. 4c and d was found to be parallel to the $(13\bar{4}0)_p$ and $(12\bar{3}0)_p$ planes, respectively. Thus, two kinds of orientation relationships between matrix and precipitate were obtained as follows.

$$[001]_m \,//\, [0001]_p \quad \text{and} \quad (010)_m \,//\, (13\bar{4}0)_p \qquad (1)$$

$$[001]_m \,//\, [0001]_p \quad \text{and} \quad (010)_m \,//\, (12\bar{3}0)_p \qquad (2)$$

The relationships are represented by the stereographic projections of Fig. 5a and b, respectively. Each of the relationships represents one of the variants of the orientation relationships between the matrix and the precipitate.

The SADPs for a precipitate were also obtained from the beam direction parallel to the $\langle 110\rangle_m$ and $\langle 111\rangle_m$ directions to confirm the orientation relationships. Figs 6 and 7 show the SADPs obtained from the beam directions of just or near $[\bar{1}10]_m$ and $[\bar{1}11]_p$ directions, respectively. In Fig. 3b for the $[\bar{1}10]_m$ zone axis, the precipitates appear parallel to the $[001]_m$ and $[\bar{1}10]_m$ directions. The diffraction patterns in Fig. 6 were obtained from precipitates aligned parallel to the $[001]_m$ direction in Fig. 3b. Fig. 6a and b are obtained from a precipitate having the orientation relationships (1) and (2) with the matrix, respectively. The both patterns are indexed in Fig. 6c.

In case of the relation (1), the angle between the $[\bar{1}10]_m$ and $[\bar{1}2\bar{1}0]_p$ directions about the axis of $[0001]_p$ // $[001]_m$ is 1.1°. In hexagonal crystal system, $[uv{\cdot}0]$ direction is orthogonal to $(uv{\cdot}0)$ plane.

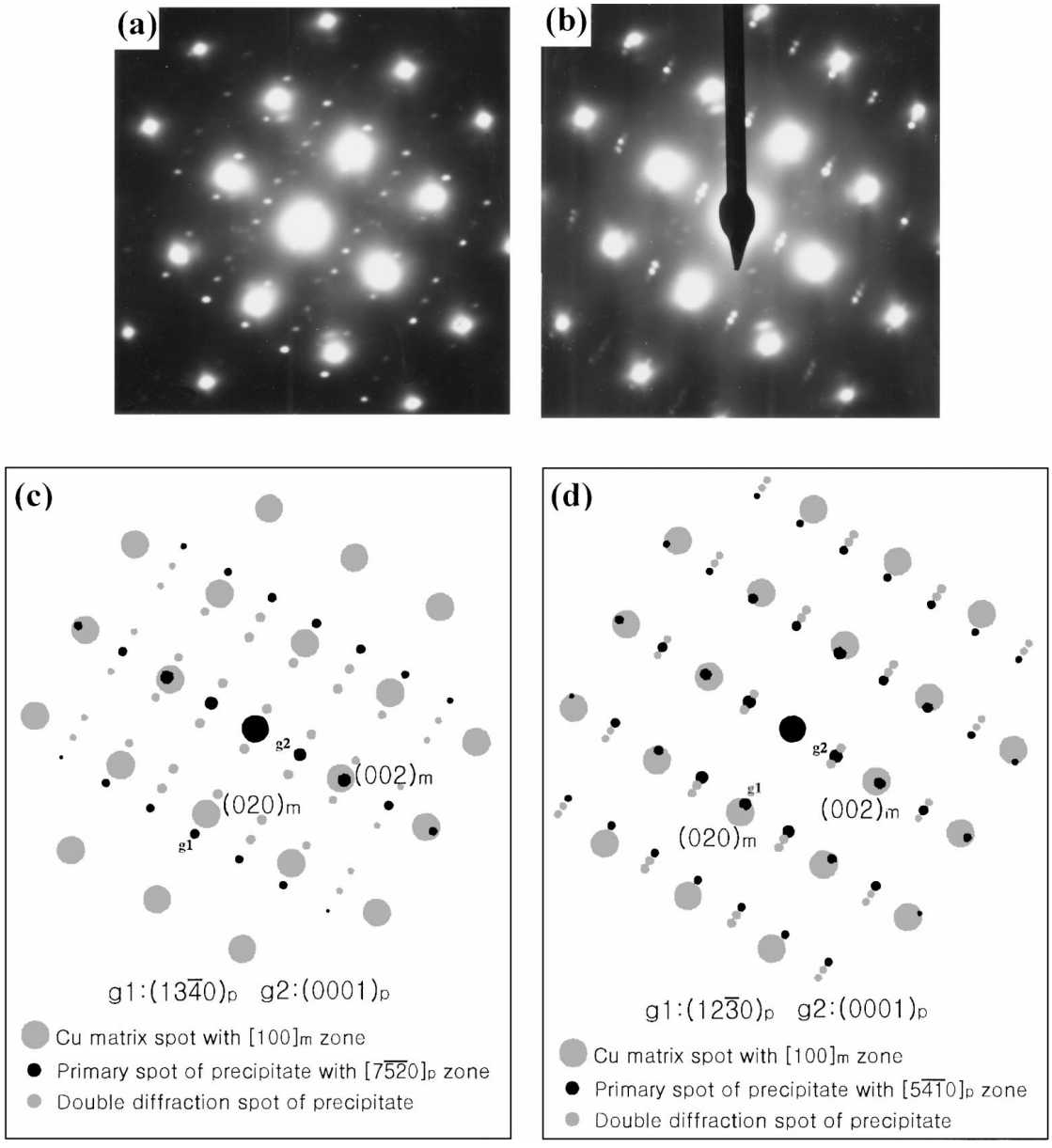


*Figure 4* SADPs of precipitate in specimen aged at 723 K for 500 h taken with $[100]_m$ zone axis parallel to (a) $[7\bar{5}\bar{2}0]_p$ and (b) $[5\bar{4}\bar{1}0]_p$. Fig. (c) and (d) are analyses of diffraction patterns of (a) and (b), respectively.

Therefore, the precipitate pattern for the $[\bar{1}2\bar{1}0]_p$ zone axis was tilted by about 1° about the axis of $[0001]_p$ // $[001]_m$ in Fig. 6a obtained for the $[\bar{1}10]_m$ zone axis.

In case of the relation (2), the angle between $[\bar{1}10]_m$ and $[\bar{1}2\bar{1}0]_p$ about the axis of $[00\bar{0}1]_p$ // $[001]_m$ is 4.1°. Therefore, the matrix pattern for $[\bar{1}10]_m$ zone was tilted by about 4° about the $[001]_m$ direction in Fig. 6b obtained for the $[\bar{1}2\bar{1}0]_p$ zone axis. The tilting angle was obtained from the Kikuchi pattern of the matrix.

The diffraction patterns in Fig. 7a and b were obtained from the precipitates along the $[\bar{1}\bar{1}2]_m$ and $[\bar{1}2\bar{1}]_m$ or $[\bar{2}11]_m$ directions in Fig. 3c, respectively. The beam directions are near $[\bar{1}\bar{1}1]_m$ direction. Fig. 7c and d show the analyses of the SADPs in Fig. 7a and b, respectively. Any simple orientation relationships between the diffraction patterns from the matrix and the precipitate could not be observed from these patterns as expected from the orientation relationships of (1) and (2).

The SADPs obtained from the precipitates in Fig. 2a and b are shown in Fig. 8a and b, respectively. Several precipitates were contained in an objective aperture. Streaks in the figures can arise because of modifications to the shape of reciprocal lattice points arising from either the shape of crystal defects or the lattice strain associated with them [23]. Discs of intensity orthogonal to the rod axis can arise from rod-shaped precipitate with small dimension.

The streaks in Fig. 8a are orthogonal to the rod axis along the $[0001]_p$ direction. This can be understood indirectly from the diffraction patterns in Fig. 4. The patterns in Fig. 4 do not show streaks, because the precipitates in Fig. 3 from which the patterns in Fig. 4 were obtained are thought to be too big to give rise to streaks. The streaks run through spots forming a cross-grid because of the high density and small dimension of precipitates and the dynamical diffraction effects. Streaking in Fig. 8b obtained from the incident beam parallel to $\langle 111\rangle_m$ can also be similarly explained.

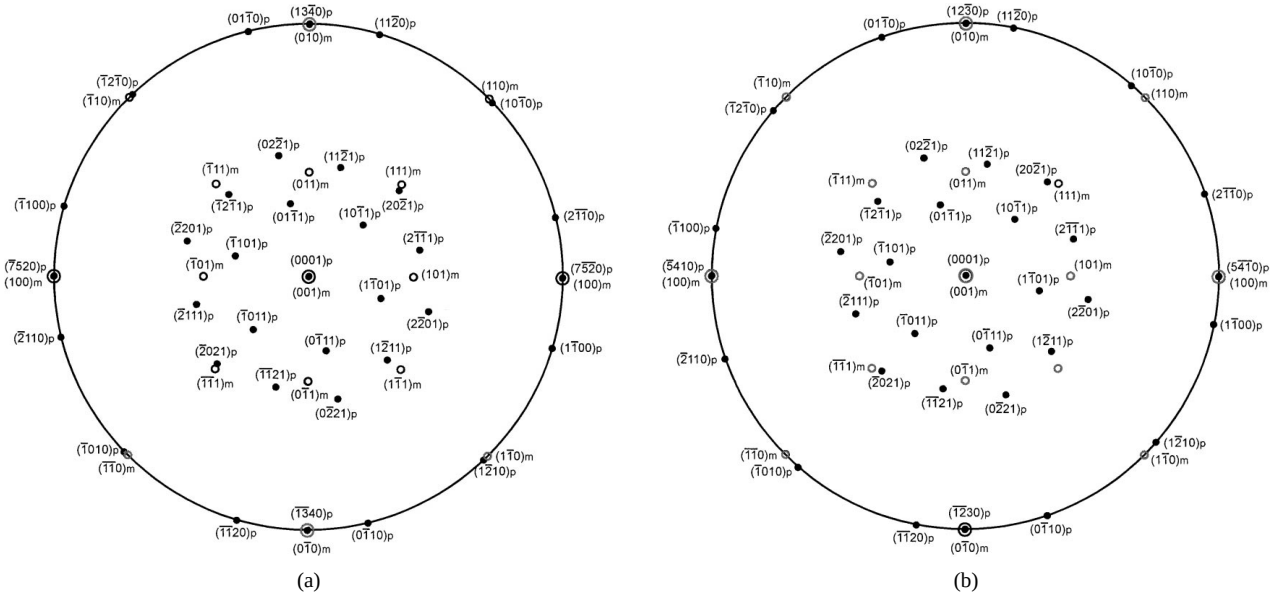


*Figure 5* Superimposed stereographic projections showing orientation relations of (a) (1) and (b) (2) between matrix and precipitate.

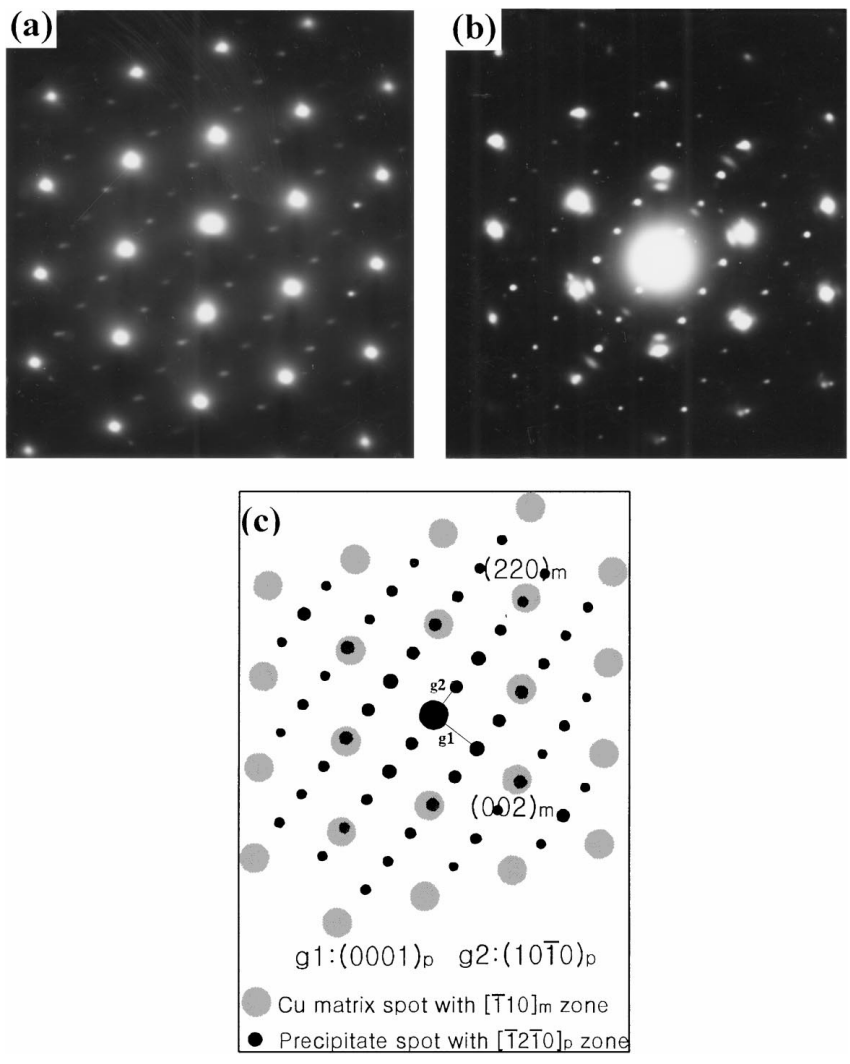


*Figure 6* SADPs of precipitate in specimen aged at 723 K for 500 h taken from (a) just and (b) near $[\bar{1}10]_m$ zone axes and (c) analysis of diffraction patterns.

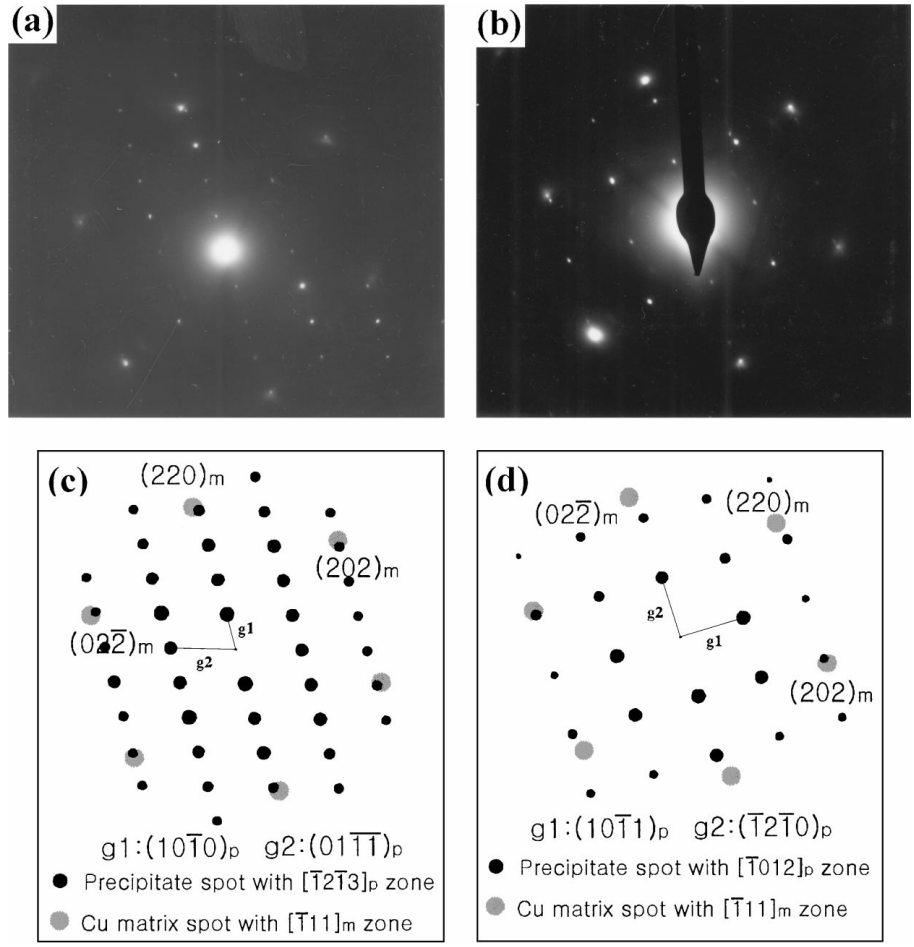


*Figure 7* SADPs of precipitate in specimen aged at 723 K for 500 h taken from near $[\bar{1}11]_m$ zone axis with (a) $[\bar{1}2\bar{1}3]_p$ and (b) $[\bar{1}012]_p$ zone axes. Fig. (c) and (d) are analyses of diffraction patterns of (a) and (b), respectively.

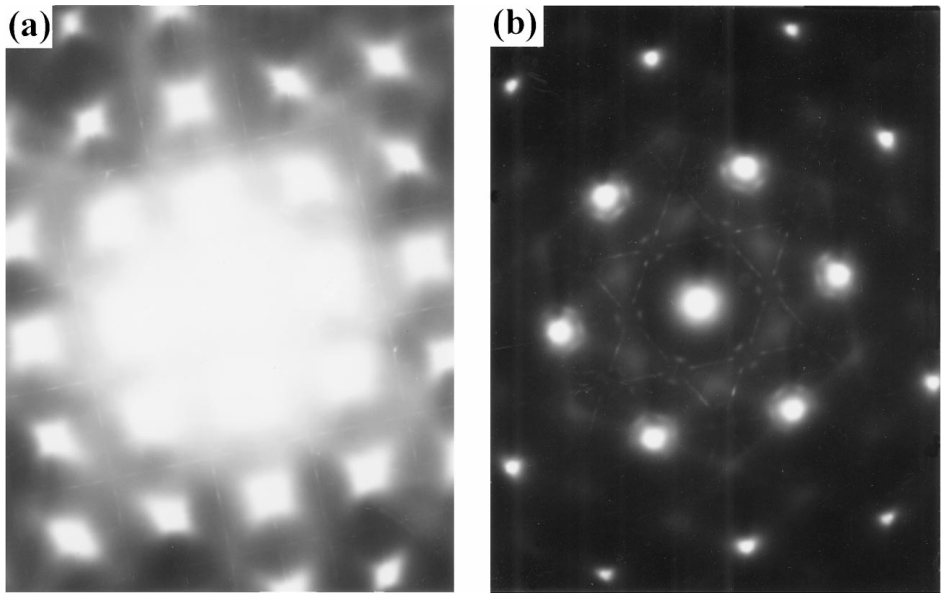


*Figure 8* SADPs of specimen aged at 723 K for 4 h obtained from (a) $[100]_m$ and (b) $[\bar{1}11]_m$ zone axes.

## 4. Conclusions

The precipitates in the aged Cu-1.11Mn-0.28P alloy are a rod-shaped compound $Mn_2P$ of a hexagonal structure. The axial orientation of the precipitates is the $[0001]_p$ direction and is parallel to the $\langle 001\rangle_m$ directions of matrix. Two different orientation relationships between the matrix and the precipitate exist as follows:

$$[001]_m // [0001]_p \text{ and } (010)_m // (13\bar{4}0)_p$$
$$[001]_m // [0001]_p \text{ and } (010)_m // (12\bar{3}0)_p$$

## Acknowledgement

This study was financially supported by the Ministry of Commerce, Industry and Energy of Korean Government and LG Metals Corporation.

## References

1. L. E. TANNER, *Phil. Mag.* **14** (1966) 111.
2. S. YAMAMOTO, M. MATSUI and Y. MURAKAMI, *Mater. Trans. JIM* **12** (1971) 159.
3. H. TSUBAKINO and R. NOZATO, *J. Jpn. Inst. Metals* **43** (1979) 42.
4. A. ROTEM, D. SHECHTMAN and A. ROSEN, *Metall. Trans.* **19A** (1988) 2279.
5. A. A. TSENG, K. P. JEN, T. C. CHEN, R. KONDETIMMAMHALLI and Y. V. MURTY, *Metall. Mater. Trans.* **26A** (1995) 2111.
6. J. SZABLEWSKI and R. HAIMANN, *Mater. Sci. Tech.* **1** (1985) 1053.
7. T. KAMIJO, H. FUKUTOMI, S. OGINO and T. SHIMIZU, *J. Jpn. Inst. Metals* **51** (1987) 569.
8. T. YAMANE, M. YASUNAGA, K. HIRAO, S. YAMASAKI, K. KAZAMA, K. YOSHIDA, R. TAKEDA and M. HIRATANI, *J. Mater. Sci.* **23** (1988) 305.
9. M. J. SAARIVIRTA, *Trans. AIME* **218** (1960) 431.
10. D. ZHILLI, A. SEKIYA, W. FUJITANI and S. HORI, *J. Jpn. Inst. Metals* **53** (1989) 672.
11. M. G. CORSON, *Proc. Inst. Met. Div. AIME* **75A** (1927) 435.
12. Y. G. KIM, T. Y. SEONG, J. H. HAN and A. J. ARDELL, *J. Mater. Sci.* **21** (1986) 1357.
13. S. A. LOCKYER and F. W. NOBLE, *ibid.* **29** (1994) 218.
14. H. FUJIWARA, T. SATO and A. KAMIO, *J. Jpn. Inst. Metals* **62** (1998) 301.
15. Y. KONISHI, T. KASHIBUCHI and F. SAKAKIBARA, *ibid.* **7** (1943) 95.
16. T. TAKAHASHI, A. KAMIO, T. MURAKAMI and T. TUZUKU, *J. Jpn. Copper Brass Res. Assoc.* **20** (1981) 128.
17. H. FUJIWARA, T. SATO and K. NAKANO, *ibid.* **30** (1991) 106.
18. H. FUJIWARA, T. SATO and A. KAMIO, *J. Jpn. Inst. Metals* **59** (1995) 502.
19. D. K. CRAMPTON, H. L. BURGHOFF and J. T. STACY, *Trans. AIME* **137** (1940) 354.
20. J. MIYAKE and M. E. FINE, *Scripta Metall.* **25** (1991) 1573.
21. J. MIYAKE, G. GHOSH and M. E. FINE, *MRS Bulletin* **21** (1996) 13.
22. J. H. CHOI, J.-S. BYUN and D. N. LEE, *J. Kor. Inst. Met. & Mater.* **37** (1999) 917.
23. J. W. EDINGTON, "Practical Electron Microscopy in Materials Science, Vol. 2" (PHILIPS, Eindhoven, 1974) p. 67.

*Received 19 May 1999*
*and accepted 3 February 2000*